Journal of Catalysis 271 (2010) 209–219

Contents lists available at ScienceDirect

Journal of Catalysis

journal homepage: www.elsevier.com/locate/jcat

Ethane dehydrogenation on Pt/Mg(Al)O and PtSn/Mg(Al)O catalysts

Vladimir Galvita, Georges Siddiqi, Pingping Sun, Alexis T. Bell *

Department of Chemical Engineering, University of California, Berkeley, CA 94720-1462, USA

ARTICLE INFO

Article history:
Received 9 October 2009
Revised 22 December 2009
Accepted 15 January 2010
Available online 21 February 2010

Keywords:
Platinum
Tin
Hydrotalcite
Mg(Al)O
Dehydrogenation
Alkanes
Alkenes

ABSTRACT

The dehydrogenation of ethane to ethene on Sn-promoted Pt supported on calcined hydrotalcite, PtSn/Mg(Al)O, was investigated with the aim of understanding the effects of Sn on the local environment of the dispersed Pt, the catalyst activity and selectivity for dehydrogenation, and the formation of coke. The origins of methane, the primary byproduct of ethane dehydrogenation were also investigated as a part of this study. Pt/Mg(Al)O was reacted with tetra-*n*-butyl tin in order to introduce Sn selectively to the dispersed Pt particles. High-resolution TEM revealed the formation of a PtSn bimetallic phase upon introduction of Sn. The activity of PtSn/Mg(Al)O for ethane dehydrogenation at 873 K was highest for a Sn/Pt ratio of 0.3, whereas the ethene selectivity increased monotonically with increasing Sn/Pt ratio, reaching 100% for Sn/Pt = 0.4. Sn promotion also significantly decreased the deposition of coke. Addition of H_2 to the feed enhanced the formation of ethene for H2/C2H6 ratios up to 0.58 for Pt/Mg(Al)O and 0.25 for PtSn/Mg(Al)O, but for higher ratios the product concentration of ethene decreased and approached that determined thermodynamically. The ethene selectivity decreased dramatically with increasing H_2/C_2H_6 ratio for Pt/Mg(Al)O but only slightly for PtSn/Mg(Al)O. Coke formation was suppressed considerably by H_2 addition to the feed, particularly for PtSn/Mg(Al)O. Isotopic tracer studies revealed that methane formation resulted primarily from the readsorption of ethene. A mechanism is proposed for ethane dehydrogenation and is used to interpret the effects of Sn promotion and the addition of H_2 to the feed.

1. Introduction

Thermal dehydrogenation of ethane on supported Pt has been investigated extensively as a means for producing ethene and hydrogen [1–3]. Since the reaction is endothermic, high temperatures are required to achieve reasonable conversions. To maintain high activity, metal sintering and coke accumulation must be minimized, and to achieve high ethene selectivity, the conversion of ethane to methane must be minimized. Previous studies have shown that non-acidic supports such as K–L zeolite, alkali-doped alumina, spinels, and calcined hydrotalcite [Mg(Al)O] minimize the adsorption of ethene and the formation of coke [4–6]. Of these supports, Mg(Al)O is particularly attractive because it is moderately basic and exhibits high thermal stability to steam and reaction-oxidation cycling [5,7–10] The addition of Sn to Pt further suppresses coking as well as minimizing metal sintering and suppressing methane formation [2,5–13]. The influence of Sn on Pt has been attributed to both geometric and electronic effects. Reduction in the size of Pt clusters present at the surface of the metal particles caused by the addition of Sn reduces the ability of Pt to cleave C–C bonds leading to the formation of CH_x species that undergo hydrogenation to methane or further dehydrogenation leading to coke [14–21]. Quantum chemical studies suggest that the presence of Sn at the surface of Pt enhances the dissociative adsorption of ethane but suppresses the adsorption of ethene [22–25]. The inclusion of hydrogen, hydrogen and oxygen, steam, or carbon dioxide has also been reported to enhance the stability of PtSn bimetallic catalysts, primarily by suppression of coke formation [26–29].

Given the wide array of roles Sn plays in modifying Pt, a considerable number of studies have been conducted to characterize the environment of Pt and Sn in Pt–Sn catalysts. EXAFS studies have demonstrated the existence of Pt–Sn interactions, but the extent of Sn interactions is shown to be highly dependent on synthesis methods [15,21,30]. XPS, focusing on Sn, has confirmed the presence of Sn(0) on catalysts, with the amount of metallic tin being dependent on the support used [4,9,15,21,31]. Mössbauer spectroscopy has been used to confirm the presence of not only Sn(0) but also Pt–Sn alloys [32–34]. Finally, HRTEM and the associated techniques of EDX and microdiffraction have also been used to identify Pt–Sn alloys [35–37].

It is notable that while much is known about the effects of Sn on the behavior of PtSn bimetallic catalysts for the dehydrogenation of ethane, there remain a number of issues not fully understood. These include the origins of coke formation, the role of coke in altering ethene selectivity, the origins of methane formation, and

* Corresponding author. Fax: +1 510 642 4778.
E-mail address: bell@cchem.berkeley.edu (A.T. Bell).

0021-9517/$ - see front matter © 2010 Elsevier Inc. All rights reserved.
doi:10.1016/j.jcat.2010.01.016

the influence of catalyst regeneration on its activity, selectivity, and stability for ethene formation. The role of Sn/Pt ratio on the catalyst activity, selectivity, and stability is also not well established. Likewise, the extent to which a PtSn bimetallic phase is formed has not been fully established. The present investigation was undertaken with the aim of addressing these issues. Studies were carried out using well-characterized Pt/Mg(Al)O and PtSn/Mg(Al)O catalysts containing the same loading of Pt in order to fully understand the role of Sn.

2. Experimental

2.1. Catalyst preparation

Hydrotalcite was prepared by the method of coprecipitation [5]. A solution containing 233.24 g of $Mg(NO_3)_2{\cdot}6H_2O$ (Alfa Aesar, 98–102%), 34 g of $Al(NO_3)_3{\cdot}9H_2O$ (Alfa Aesar, 98–102%) dissolved in 1000 mL deionized H_2O was mixed dropwise with a solution containing 4.8 g of Na_2CO_3 (EMD Chemicals Inc., 99.5%) and 45.32 g of NaOH (Fisher Scientific, 98.3%) dissolved in 1000 ml H_2O. Co-precipitation was carried out with stirring at 333 K for 1 h. The precipitate was filtered and dried overnight at 383 K. The dried material was then heated in air at 2 K/min up to a temperature of 973 K. The calcined material is referred to from here on out as Mg(Al)O. The BET surface area of the dried hydrotalcite was 300 m^2/g, but after calcination the surface area of Mg(Al)O decreased to 200 m^2/g. The Mg/Al ratio of Mg(Al)O determined by elemental analysis was five.

Prior to impregnation with Pt and Sn, the Mg(Al)O support was dried at 473 K for 2 h in air. Pt was introduced by mixing the support with three pore volumes of a solution containing Pt(acetylacetonate)$_2$ (Sigma Aldrich, 99.99%) dissolved in toluene (2.7 mL toluene/g catalyst). The Pt content varies from 0.7 wt.% to 0.8 wt.% [38]. The mixture was then stirred until it became powdery, left at room temperature in air for 2 h, and then dried at 383 K in air for 4 h. After drying, the catalyst was reduced at 723 K for 2 h (5 K/min temperature ramp) in a flow of 10% H_2/Ar (60 cm^3/min) [15]. The resulting material was either kept for characterization or transferred immediately (exposure to air at room temperature was limited to <1 min) to the reaction vessel for further impregnation with Sn. Tetra-*n*-butyl tin was used as a precursor instead of $SnCl_2$ in order to achieve a preferential reaction of the precursor with the Pt particles and dispersed on the support and to avoid leaching of Mg from the support, an effect observed when samples were prepared using $SnCl_2$. The amount of tetra-*n*-butyl tin used was varied based on the Sn/Pt ratio (for $0 < Sn/Pt < 1$) desired for the catalyst, a complete reaction of the tin precursor with the Pt clusters was assumed, this was confirmed with inductively coupled plasma optical emission spectroscopy (ICP-OES). Tin was introduced by mixing Pt/Mg(Al)O with a solution of tetra-*n*-butyl tin (Alfa Aesar, 94%) in decane (10 mL solvent/g support) under an flowing 10% H_2/Ar atmosphere (120 cc/min) [39]. To create catalysts with $Sn/Pt \sim 1$, an excess of tetra-*n*-butyl tin was used corresponding to Sn/Pt = 2. The reaction vessel was then sealed and 120 cm^3/min of 10% H_2/Ar was continuously flowed while heating to 358 K for 4 h with stirring. After reaction, the wet powder was extracted and washed with decane and vacuum dried in air [38,40]. The vacuum dried material was then reduced under 10% H_2/Ar (60 cc/min) for 2 h at 383 K, 1 h at 623 K, and 1 h at 873 K (5 K/min ramp rate). The resulting PtSn bimetallic catalyst was re-reduced *in situ* immediately prior to catalyst testing.

2.2. Catalyst characterization

The structure of the support was characterized before and after calcination by X-ray powder diffraction (XRD) on a Siemens Diffractometer D 5000 with Cu Kα radiation (λ = 1.5418 Å) at 20 kV and 5 mA. The samples were scanned from 5° to 70° 2θ with a step size of 0.02° and a dwell time of 1.0 s. Thermogravimetric analysis (TGA) and differential scanning calorimetry (DSC) of the as-prepared support were carried out using a TA instrument, SDT 2960 Simultaneous DSC–TGA. About 20–30 mg of as-synthesized hydrotalcite, was placed in alumina crucible that was heated from 303 K to 1273 K at a rate of 10 K/min in the TGA–DSC instrument nitrogen flowing at 100 cm^3/min. The surface area of as-synthesized and calcined supports was determined by multi-point method using an Autosorb-1 instrument (Quantachrome Corporation, Boynton Beach, FL). Prior to measurement of surface area, each sample was degassed at 573 K for 22–24 h. The Pt, Mg, Al, Sn contents of the support and of support Pt and Pt/Sn were determined by Galbraith Laboratories (Knoxville, TN) using ICP-OES. The dispersion of Pt on Pt/Mg(Al) O was determined by H_2 chemisorption using a AutoChem II 2920 (Micromeritics Instrument Corporation). About 60 mg of Pt/Mg(Al)O was loaded into a quartz cell and then reduced in flowing 10% H_2/Ar (50 cm^3/min). The temperature of the sample was raised at 5 K/min to 873 K and then maintained at this level for 2 h. The sample was then flushed in flowing Ar for 90 min and then cooled down to 308 K. The pulse size was 50 cm^3/g and the time between pulses was 10 min.

Raman spectra were recorded with a Kaiser Optical HoloLab series 5000 Raman spectrometer equipped with a Nd:YAG laser that is frequency-doubled to 532 nm. The laser was operated at a power level of 25 mW measured at the sample with a power meter. A Princeton Instruments TEA/CCD detector was operated at −40 °C. Spectra were recorded with a resolution of 2 cm^{-1}. Samples (approximately 25 mg each) were pressed into pellets at 5000 psi and placed within a rotary quartz Raman cell. The samples were rotated at 100 rpm during the measurements to reduce the effects of sample heating by the laser. A quartz reactor allowed the sample to be heated and reacted with gases while gathering Raman spectra.

Analysis of the samples by transmission electron microscopy (TEM) was carried out at the Electron Microscopy Lab at UC Berkeley using a FEI Tecnai 12 Transmission electron microscope. High-resolution TEM studies were conducted at the National Center for Electron Microscopy (NCEM), at the Lawrence Berkeley National Lab using the OAM microscope, which is a modified Philips CM300FEG/UT. Samples were prepared by suspending ~5 mg of sample in ethanol, dripping the solution onto a 200-mesh Cu grid coated in holey carbon (SPI Supplies, West Chester, PA, USA), and letting the ethanol evaporate. HRTEM images were obtained using the Scherzer focus, then defocusing the microscope and taking a series of images with varying degrees of defocus. Images were reconstructed from the series of defocused images via exit wave reconstruction, using the MACTEMPAS software at NCEM. Analysis of the reconstructed images was done using MACTEMPAS and CrystalKit to analyze the FFT images and determine the crystal structure [41].

2.3. Catalyst testing

Reactions were carried out in a quartz reactor with an inner diameter of 7 mm. Prior to testing, the catalyst (0.025 g, 0.25–0.5 mm particle size, diluted with quartz particles of the same particle size in a 1:4 ratio) was heated at 10 K/min to 883 K in 10% H_2 in He and then maintained at this temperature for 1.5 h. The catalyst bed was heated by a three-zone furnace (Applied Test System, Inc.) controlled by Watlow 988 controllers. The temperature of the catalyst bed was measured by two thermocouples centered axially inside the reactor, one at the top and one at the bottom of the catalyst bed. Brooks Mass Flow Controllers (MFC) were used to deliver a defined flow of each gas. The feed concentrations were varied

from 2% to 30% for ethane and from 0% to 25% for hydrogen. For residence time experiments, the amount of catalyst was varied from 10–25 mg for Pt/Mg(Al)O and 10–50 mg for PtSn/Mg(Al)O, and flowrates varied from 0.25 to 3 cm^3/s. All experiments were performed in the kinetic regime. Internal mass transport limitations were not observed as evidenced by a linear Arrhenius plot. Catalyst deactivation due to coke deposition was observed. Regeneration of the catalysts was done by oxidizing the catalyst in a flow of 5 vol.% O_2 in He (100 cm^3/min) for 15 min and then reducing the catalyst in a flow of 20 vol.% H_2 in He (100 cm^3/min) for 30 min. Prior to the changing the gas composition, the reactor was flushed with helium. The amount of coke was determined by combustion of the deposited material. Prior to combustion, the catalyst was (0.025 g) purged in a flowing He (60 cm^3/min) at 873 K for 30 min, after which it was exposed to a mixture of 5% O_2 in He flowing at 100 cm^3/min. The CO_2 generated was monitored by an on-line mass spectrometer. The flow of O_2 was stopped once the production of CO_2 ceased. The amount of deposited coke on the catalyst was calculated from the amount of generated CO_2.

Reactants and products were analyzed on-line using a gas chromatograph–mass spectrometer (Varian, Model 320) equipped with a 14-port sampling valve and three sample loops. One sample loop was injected into an Alumina PLOT column for the FID and MS, and the other one into a Hayesep and Mol Sieve packed columns. A thermal conductivity detector (TCD) was used to measure the concentration of He and H_2. A flame ionization detector (FID) and mass spectrometer were used to measure the concentrations of all organic compounds eluting from the capillary column.

The ratio of hydrogen to ethane partial pressure in the feed was varied from 0 to 2.5, while maintaining the total flow constant by appropriate addition of He. To compensate for catalyst deactivation, measurements of ethane conversion were made after 60 min of time on stream at which time the conversion changed by less than 10%. Experiments conducted with the empty reactor showed that the conversion of ethane was less than 0.01% at 893 K.

The overall ethane conversion was calculated according to Eq. (1):

$$X_{C_2H_6}(\%) = \left(1 - F_{out}[C_2H_6]_{out}/F_{in}[C_2H_6]_{in}\right) \cdot 100\% \quad (1)$$

where F_{in}, F_{out} are inlet and outlet molar flow rate of ethane. The selectivities to ethene and methane were determined from Eqs. (2) and (3):

$$S_{C_2H_4}(\%) = [C_2H_4]/([C_2H_4] + 0.5[CH_4]) \cdot 100\% \quad (2)$$

$$S_{CH_4}(\%) = 0.5[CH_4]/([C_2H_4] + 0.5[CH_4]) \cdot 100\% \quad (3)$$

2.4. Isotopic labeling

All isotopic labeling experiments were performed at atmospheric pressure with 600 °C as a standard temperature and total flow rate 60 cm^3/min. The experiments where H_2 in the feed was replaced with D_2 were performed on Pt/Mg(Al)O and Pt–Sn/Mg(Al)O catalysts. Prior to deuterium labeling experiments, the catalyst was reduced in D_2, with a D_2 feed partial pressure of 11.3 kPa and with the ratio of partial pressures of ethane and deuterium being 0.58. Natural occurrence of 1% ^{13}C in carbon was neglected by common approximation in calculation of isotopomer distributions [42]. D_2 gas (99.9% isotopic purity) was obtained from Sigma–Aldrich. An experiment where $^{13}C_2H_4$ was cofed with unlabeled ethane to Pt–Sn/Mg(Al)O catalyst was also performed to study the origin of the byproducts and the extent of reverse reactions. Experiments were carried out at different ratios of ethane and hydrogen ($H_2/^{13}C_2H_6$ = 1.25, 0.58, and 0). Prior to ^{13}C isotopic labeling experiments, the reactor was flushed with ethane-free flow to avoid contamination with unlabeled ethane. No kinetic isotope effect was expected in ^{13}C labeling experiments. $^{13}C_2H_4$ gas (99 atm.% ^{13}C) was obtained from Sigma–Aldrich. The isotopic composition of reagents and products was determined by using a Varian gas chromatograph–mass spectrometer.

3. Results

3.1. Catalyst characterization

Fig. 1 shows XRD patterns for the support taken after synthesis and after calcination. The positions of the diffraction lines observed after synthesis are consistent with those reported for hydrotalcite [43]. The BET surface area of the as-synthesized support is 300 m^2/g. Fig. 2A shows a TEM image of the support prior to calcinations. A rag-like, layered structure is evident, consistent with the structure of hydrotalcite. TGA–DSC analysis shows that water is evolved at 373 K and 643 K, and carbon dioxide at 353 K and 623 K. The XRD pattern of the calcined support shows two lines characteristic of cubic MgO. The Al present in the original hydrotalcite is believed to be retained and located in interstitial sites in the MgO framework after calcination [44]. Calcination led to a reduction in the BET surface area to 200 m^2/g. Consistent with the loss in surface area, the TEM image of the calcined support shows denser plate-like structures (Fig. 2B).

The introduction of Pt and then Sn did not lead to a loss in the surface area of the calcined support. The BET surface area remained at 200 m^2/g, and the image of the support shown in Fig. 2B is similar to that seen in Fig. 2A prior to calcinations. Small particles of Pt and PtSn are evident in Fig. 2C and D. The average diameter of these particles was 1.0–1.5 nm. This corresponds well to the mean particle size calculated from the Pt/Mg(Al)O dispersion of 84%, determined by H_2 chemisorption, of 1.35 nm, calculated from dispersion of Pt. Formation of PtSn bimetallic particles is clearly evident from high-resolution TEM. Fig. 3A shows a HRTEM image obtained via exit wave reconstruction of a series of defocused images taken for an as-prepared sample of the catalyst having a Sn/Pt ratio of 0.23. The bright spots presenting this image represent atoms. The indicated reflections in the FFT of the particle (Fig. 3B) have spacings in reciprocal lattice space of 0.28 $Å^{-1}$, 0.34 $Å^{-1}$, and 0.37 $Å^{-1}$, which correspond well to the first three (0 1 0), (0 1 1), and (0 0 2), reflection planes of PtSn [45]. The reflections planes observed have far smaller lattice spacings than those observed for Pt, which has its first (1 1 0), reflection plane at 0.44 $Å^{-1}$. It is noted that particles of Pt, and possibly Pt-rich PtSn alloys, should coexist with particles of PtSn, since the Sn/Pt ratio of the sample examined was less than 1.0. However, definitive identification of such Pt-rich phases could not be made because the majority of the observed particles were so small (~1.5 nm) that diffraction patterns of sufficient quality to differentiate the Pt phase from the support phase could not be obtained.

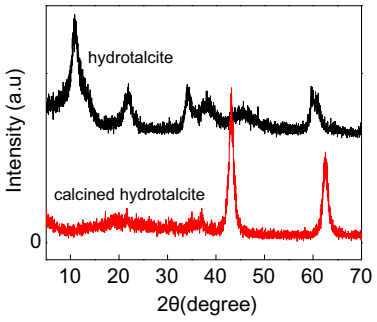

Fig. 1. XRD patterns for as-prepared and calcined hydrotalcite.

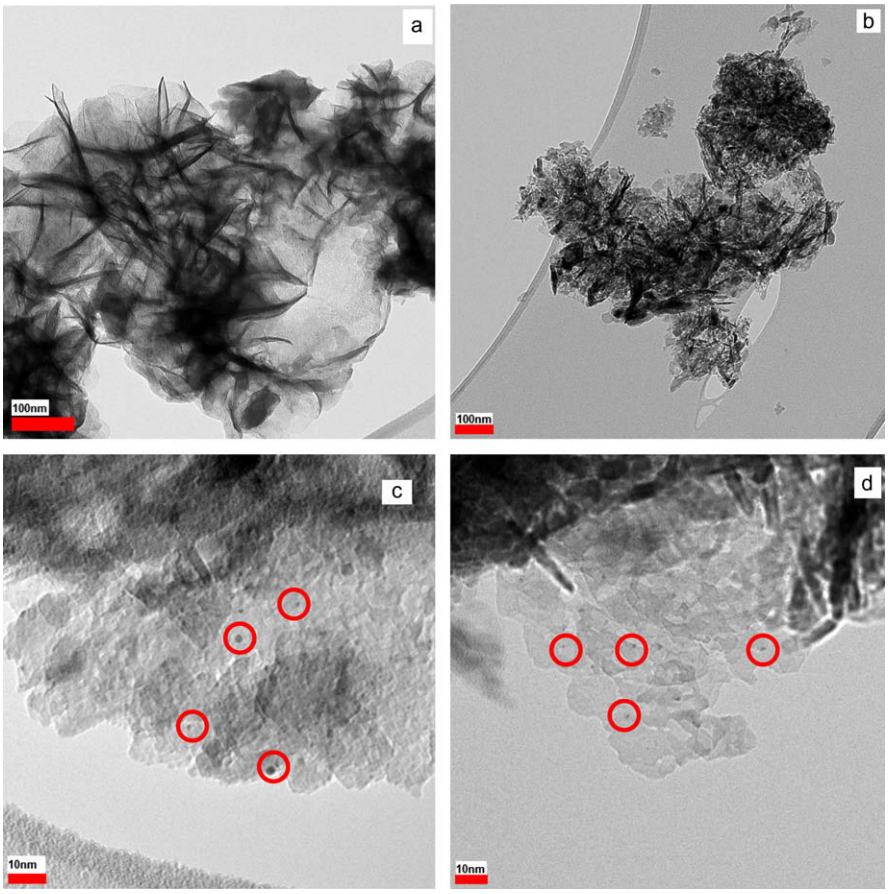

Fig. 2. TEM images of (a) as-prepared hydrotalcite, (b) hydrotalcite calcined at 973 K, (c) Pt/Mg(Al)O, and (d) PtSn/Mg(Al)O. The circled spots in images (c) and (d) show areas where Pt or Pt bimetallic particles are present.

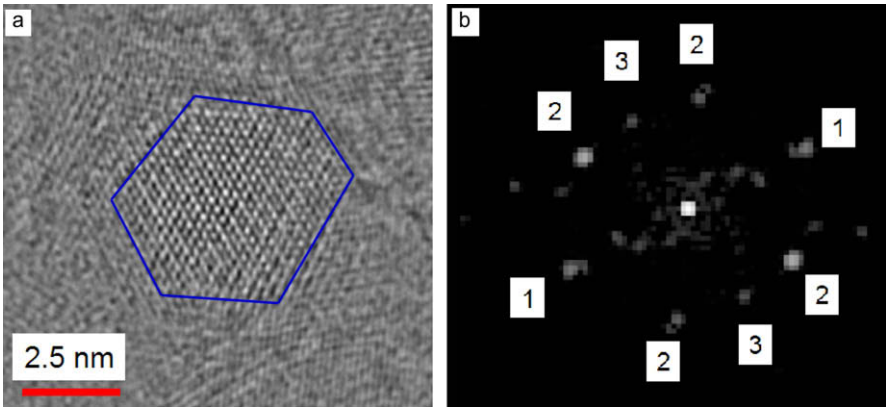

Fig. 3. (a) PtSn/Mg(Al)O, Sn/Pt = 0.23, as-prepared, HRTEM image (b) Hanning masked FFT of the particle, inverse lattice spacings for points: (1) 0.37 $Å^{-1}$, (2) 0.34 $Å^{-1}$, and (3) 0.28 $Å^{-1}$.

3.2. Catalytic performance of Pt/Mg(Al)O and PtSn/Mg(Al)O

Pt/Mg(Al)O and PtSn/Mg(Al)O were active for ethane dehydrogenation over the range of 823–873 K. Evidence for homogeneous dehydrogenation was observed above 873 K, so higher temperatures were not investigated. The apparent activation energy for ethane dehydrogenation over the range investigated was calculated to be 114 kJ/mol and 102 kJ/mol for Pt/Mg(Al)O and PtSn/Mg(Al)O, respectively. Based on the results of these preliminary studies, all further experiments were conducted at 873 K.

Fig. 4 shows the conversion of ethane to ethene and the selectivity to ethene for Pt/Mg(Al)O and PtSn/Mg(Al)O as functions of time. The reaction conditions used for both catalysts were the same: the ethane inlet concentration was 19.5%, the total gas flow rate was 60 cm^3/min, the reaction temperature was 873 K, and no H_2 was included in the feed. Both catalysts exhibited a rapid loss in conversion during the first 40 min of time on stream but then attained a period of nearly constant conversion. During this period, the conversion of ethane to products was 0.66% for Pt/Mg(Al)O and 2.6% for PtSn/Mg(Al)O, resulting in an activity for PtSn/Mg(A-

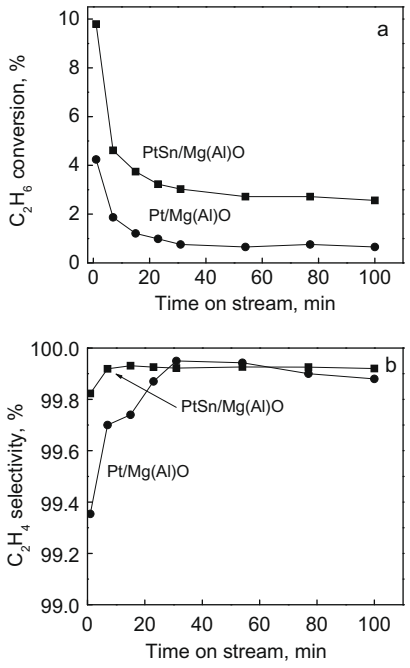

Fig. 4. Plots of C_2H_6 conversion (a) and C_2H_4 selectivity (b) versus time on stream for Pt/Mg(Al)O and PtSn/Mg(Al)O (Sn/Pt = 1.08). Reactions conditions: C_2H_6 partial pressure = 19.5 kPa; T = 873 K; Q = 60 cm^3/min.

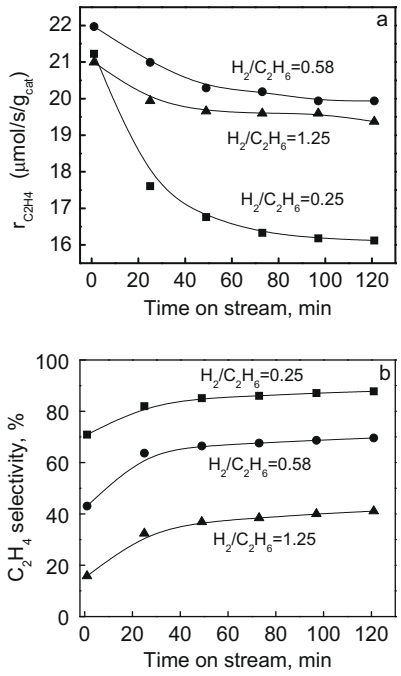

Fig. 5. Effects of H_2/C_2H_6 ratio on the (a) rate of production of C_2H_4 and (b) C_2H_4 selectivity versus time on stream for ethane dehydrogenation on Pt/Mg(Al)O at 873 K and a C_2H_6 partial pressure of 19.5 kPa and a total feed flow rate of 60 cm^3/min.

l)O that was a factor of ~3 higher than that for Pt/Mg(Al)O under identical conditions. The ethene selectivity of Pt/Mg(Al)O was 99.4% initially and then rose to 99.9%, whereas that of PtSn/Mg(Al)O was 99.8% initially and then rose to 99.9%. The only other carbon-containing product observed besides ethene was methane.

Prior studies have shown that catalyst deactivation can be inhibited by adding H_2, H_2/O_2, CO_2, or H_2O to the feed [26–29]. Figs. 5 and 6 show the effects of adding H_2 to the feed for Pt/Mg(Al)O and PtSn/Mg(Al)O, respectively. In the case of Pt/Mg(Al)O raising the ratio of H_2 to C_2H_6 from 0.25 to 1.25 strongly inhibited the loss of activity for ethene formation and increased the steady-state activity of the catalyst. However, H_2 addition to the feed also caused a significant decrease in the selectivity to ethene and a corresponding increase in the selectivity to methane relative to that observed in the absence of H_2 addition (see Fig. 5), but nevertheless the ethene selectivity rose with time on stream. H_2 addition to the feed also reduced the loss of activity for ethene formation on PtSn/Mg(Al)O but to a lesser extent than was observed for Pt/Mg(Al)O, and in contrast to what was observed with that catalyst, the activity for ethene formation decreased with increasing addition of H_2. The presence of H_2 in the feed stream also caused a loss in the selectivity to ethene for PtSn/Mg(Al)O but to much lesser extent than was observed for Pt/Mg(Al)O (see Fig. 6).

Fig. 7a and b shows the amount of carbon deposited on the catalyst as a function of time on stream and the H_2/C_2H_6 ratio in the feed. In the absence of H_2 in the feed both Pt/Mg(Al)O and PtSn/Mg(Al)O accumulated carbon rapidly with time on stream, the amount being roughly a factor of two less for PtSn/Mg(Al)O than Pt/Mg(Al)O. When H_2 is added to the feed at the level of H_2/C_2H_6 = 1.25, the amount of carbon accumulated was greatly reduced, particularly for PtSn/Mg(Al)O. Raman spectra of the catalyst taken after ethane dehydrogenation and after oxidation are shown in Fig. 8. The bands seen at 1315 and 1575 cm^{-1} are attributable to graphite-like species [46–48]. After catalyst oxidation of the used catalysts at 673 K, these bands disappeared completely (Fig. 8B).

Further evidence of the effects of H_2/C_2H_6 ratio on the activity and selectivity of ethene formation on Pt/Mg(Al)O and PtSn/Mg(Al)O

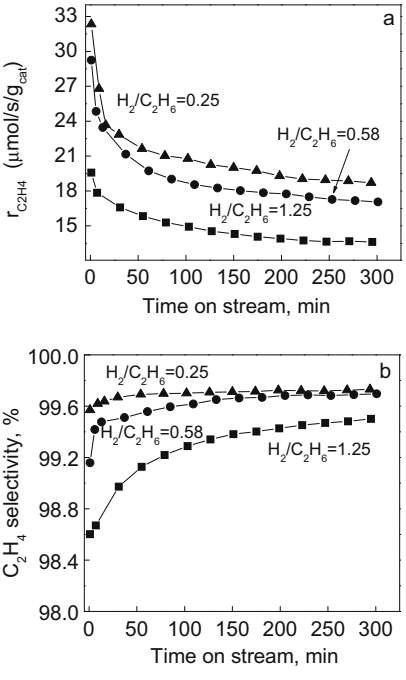

Fig. 6. Effects of H_2/C_2H_6 ratio on the (a) rate of production of C_2H_4 and (b) C_2H_4 selectivity versus time on stream for ethane dehydrogenation on PtSn/Mg(Al)O (Sn/Pt = 1.08) at 873 K, C_2H_6 partial pressure of 19.5 kPa, and a total feed flow rate of 60 cm^3/min.

is shown in Fig. 9. For both catalysts, the production of ethene, passed through a maximum and then decreased with increasing H_2/C_2H_6 ratio. At high values of H_2/C_2H_6, the rate of production of ethene approached that predicted by thermodynamic equilibrium. It is notable that the rate of formation of ethene produced by PtSn/Mg(Al)O was only slightly greater than that produced by Pt/Mg(Al)O.

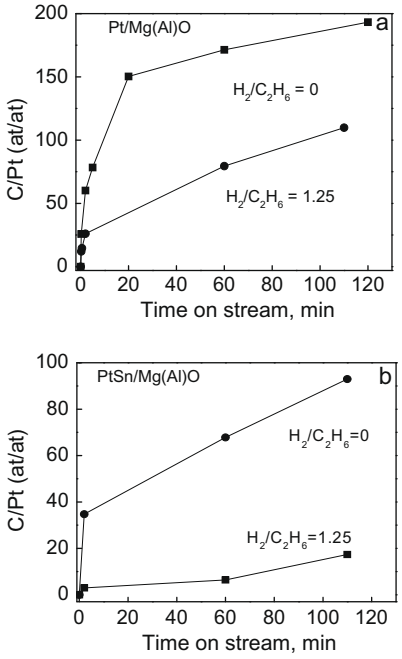

Fig. 7. Amount of coke accumulation with time on stream for ethane dehydrogenation on (a) Pt/Mg(Al)O and (b) PtSn/Mg(Al)O (Sn/Pt = 1.08) at 873 K, C_2H_6 partial pressure of 19.5 kPa, and total feed flow rate of 60 cm^3/min.

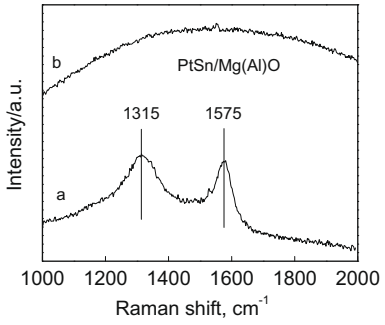

Fig. 8. Raman spectra taken (a) after dehydrogenation of ethane on PtSn/Mg(Al)O (Sn/Pt = 1.08) at 873 K with a C_2H_6 partial pressure of 19.5 kPa and a total feed flow rate of 60 cm^3/min and (b) after oxidation of reacted sample for 20 min in 10% O_2/He.

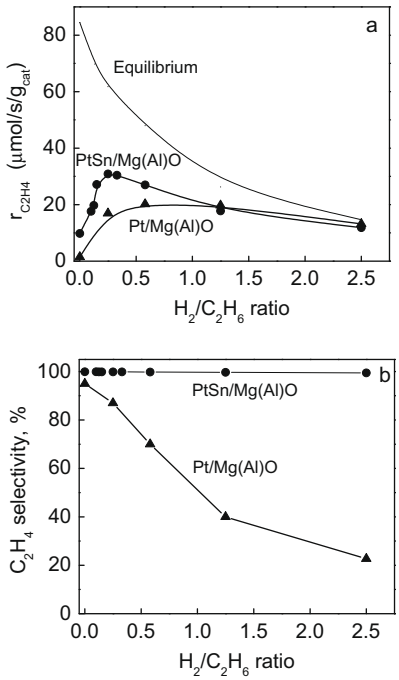

Fig. 9. Effect of H_2/C_2H_6 ratio on the (a) rate of production of C_2H_4 and (b) selectivity to C_2H_4 for ethane dehydrogenation on Pt/Mg(Al)O and PtSn/Mg(Al)O (Sn/Pt = 1.08) at 873 K with a C_2H_6 partial pressure of 19.5 kPa and a total feed flow rate of 60 cm^3/min.

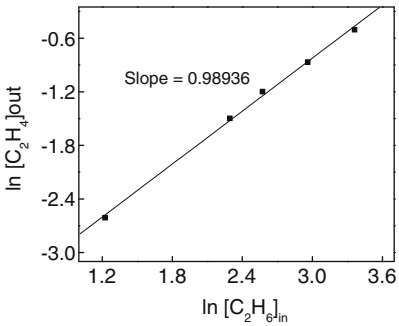

Fig. 10. Effect of ethane feed concentration on the rate of ethene formation determined for PtSn/Mg(Al)O (Sn/Pt = 1.08) at 873 K. The ethane concentration was varied from 3% to 30%, while the total concentration of H_2 in feed was maintained at 25%. He was added to maintain a constant flowrate of 60 cm^3/min.

However, the selectivity to ethene decreases from 100% to 20% as the H_2/C_2H_6 ratio increases from 0 to 2.5 for Pt/Mg(Al)O, but decreased only slightly from 100% for PtSn/Mg(Al)O over the same range of H_2/C_2H_6 ratios. Since methane was the only other hydrocarbon product produced, these results demonstrate that the formation of methane increases significantly with increasing H_2/C_2H_6 ratio for Pt/Mg(Al)O, but not for PtSn/Mg(Al)O. To study the reaction order with respect to ethane, H_2 in the feed was kept constant, and the amount of ethane was increased from 3% to 30%. Shown in Fig. 10, the ethane dehydrogenation reaction is first order with respect to ethane.

The effects of residence time on the performance of Pt/Mg(Al)O and PtSn/Mg(Al)O catalysts are shown in Fig. 11a–c. To compensate for catalyst deactivation during residence time variation experiments, the products concentration at reference conditions was measured when concentration deviations between successive measurements were not more than 5%. Fig. 11a shows that the production of ethene increased with increasing space time for both Pt/Mg(Al)O and PtSn/Mg(Al)O and that for low residence times the production of ethene from both catalysts was nearly identical. However, at higher residence times, the ethene production observed for Pt/Mg(Al)O was below that observed for PtSn/Mg(Al)O. As seen in Fig. 11b, the production of methane from Pt/Mg(Al)O at low residence times was comparable to the amount of ethene formed, but the production of methane becomes significantly higher than that of ethene at higher space residence times. Consistent with these observations, Fig. 11c shows that the selectivity to ethene falls and the selectivity to methane rises with increasing residence time. In contrast to Pt/Mg(Al)O, the selectivity to ethene remained high for PtSn/Mg(Al)O, irrespective of the residence time. The results presented in Fig. 11 clearly demonstrate that the addition of Sn to Pt/Mg(Al)O has a much larger effect on the formation of methane than on the formation of ethene. The change in ethene and methane selectivities with residence time suggests that methane may be formed both as a primary product of ethane hydrogenolysis and as a secondary product of ethene hydrogenolysis, a subject discussed in more detail in the next paragraph.

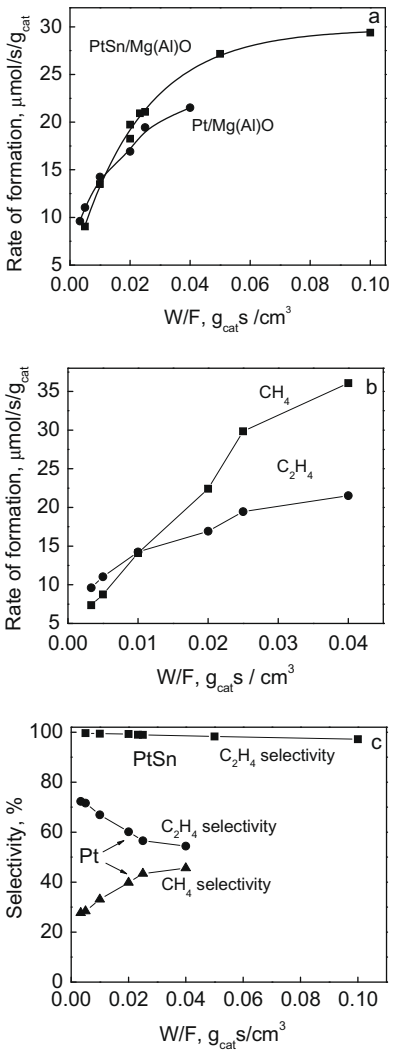

Fig. 11. Effects of W/F on the rate of formation (a) of C_2H_4 observed for Pt/Mg(Al)O and PtSn/Mg(Al)O (Sn/Pt = 1.08), (b) of C_2H_4 and CH_4 observed for Pt/Mg(Al)O, and (c) the C_2H_4 selectivity observed for Pt/Mg(Al)O and PtSn/Mg(Al)O for ethane dehydrogenation at 873 K and a feed partial of C_2H_6 of 19.5 kPa.

3.3. Isotopic labeling experiments

$^{13}C_2H_4$ was cofed with unlabeled C_2H_6 with the aim of understanding the origin of methane and the extent to which product ethene undergoes hydrogenation back to ethane. These experiments were carried out at 873 K after reduction of the catalyst in H_2. Table 1 lists the isotopomer distributions for ^{13}C-unlabled, singly labeled, and doubly labeled C_2H_4 and C_2H_6 present in the products formed on PtSn/Mg(Al)O for different H_2/C_2H_6 feed ratios. With no H_2 added to the feed none of the C_2H_6 was ^{13}C labeled. The ethane in the products was comprised of a small concentration of $^{12}C_2H_4$ and a large concentration of $^{13}C_2H_4$, but contained hardly any $^{12}CH_2{}^{13}CH_2$. Thus, in the absence of H_2 addition to the feed the $^{13}C_2H_4$ passed through reactor without significant transformation. Upon addition of H_2 to the feed the concentration of $^{12}C_2H_4$ increased progressively, consistent with what was observed in Fig. 9. The presence of H_2 in the feed also increased the concentration $^{13}C_2H_6$ at the expense of decreasing the concentration of $^{13}C_2H_4$ due to hydrogenation of the doubly labeled ethene.

The origins of methane formation were investigated with Pt/Mg(Al)O, since virtually no methane was formed on PtSn/Mg(Al)O. For these experiments, H_2 was added to the feed (H_2/C_2H_6 = 1.25) together with 1.4% $^{13}C_2H_4$. The fractional distribution of $^{13}CH_4$, $^{13}C_2H_4$, and $^{13}C_2H_6$ produced are listed in Table 2. Only 14% of the product methane was ^{13}C labeled. The principal source of product methane was deduced from the following considerations. The conversion of $^{13}C_2H_4$ to methane was 7.4% and the conversion of $^{12}C_2H_6$ to methane was 3.2%; however, it must be recognized that the partial pressure of $^{12}C_2H_6$ was 14 times higher than the partial pressure of $^{13}C_2H_4$. These observations suggest that methane formation from ethene is much more rapid than the formation of this product directly from ethane, and that $^{12}CH_4$ is produced as a secondary product from $^{12}C_2H_4$, consistent with what was inferred from Fig. 11. The fraction of $^{13}C_2H_4$ in the products was 16%, indicating that most of the product ethene derived from dehydrogenation of C_2H_6. The observation of 5.5% $^{13}C_2H_6$ in the products indicates that rehydrogenation of ethene occurs under the experimental conditions used. The conclusion that ethene is the principal source of methane is consistent with the work of Virnovskaia et al. in which $^{12}CH_3{}^{13}CH_3$ was cofed with unlabeled ethene over a PtSn/Mg(Al)O catalyst similar to that used in the present study [26].

Table 2
Isotopomer distribution observed for the dehydrogenation of C_2H_6 in the presence of $^{13}C_2H_4$ over Pt/Mg(Al)O at 873 K.

Isotopomer	Percent ^{13}C in compound
CH_4	14.4
C_2H_4	15.8
C_2H_6	5.5

Feed partial pressures – C_2H_6, 19.5 kPa; $^{13}C_2H_4$, 1.4 kPa; H_2 – 25 kPa; T = 873 K.

Table 1
Isotopomer distribution observed for the dehydrogenation of C_2H_6 in the presence of $^{13}C_2H_4$ and the hydrogenation of $^{13}C_2H_4$. For both reactions, the catalyst is PtSn/Mg(Al)O and the reaction temperature is 873 K.

H_2/C_2H_6[a]	Compound	Measured isotopomer distributions [C_i] (vol.%)		
		$^{12}C^{12}C$	$^{12}C^{13}C$	$^{13}C^{13}C$
1.25	C_2H_4	1.25	0.02	0.93
	C_2H_6	16.7	0.01	0.62
0.58	C_2H_4	1.46	0.03	1.11
	C_2H_6	16.24	0	0.42
0	C_2H_4	0.39	0.02	1.53
	C_2H_6	17.66	0	0
*H_2/C_2H_4 = 1[b]	C_2H_4	0	0.01	1.25
	C_2H_6	0	0.01	0.39

[a] Feed partial pressures – C_2H_6 = 19.5 kPa, $^{13}C_2H_4$ = 1.65 kPa, H_2/C_2H_6 = 0–1.25.
[b] Feed partial pressures – $^{13}C_2H_4$ = 1.65 kPa; H_2 = 1.65 kPa.

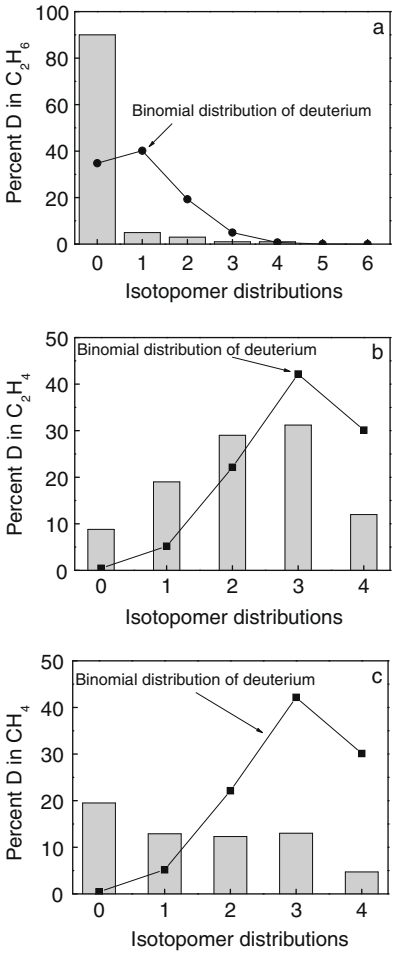

Fig. 12. Isotopomer distribution of (a) $C_2H_xD_{6-x}$, (b) $C_2H_xD_{4-x}$, and (c) CH_xD_{4-x} observed during ethane dehydrogenation in the presence of D_2 over Pt/Mg(Al)O at 873 K with a C_2H_6 partial pressure of 19.5 kPa, a D_2 feed partial pressure of 11.3 kPa, and a total flow rate of 60 cm^3/min.

Experiments were carried out in which D_2 was fed together with C_2H_6 over both Pt/Mg(Al)O and PtSn/Mg(Al)O with the objective of establishing the effect of catalyst composition on the extent of H/D exchange. The level of exchange observed for the empty reactor at 873 K was only 1%. Fig. 12 shows the deuterium distribution in ethane, ethene, and methane during the reaction of a C_2H_6/D_2 mixture over Pt/Mg(Al)O catalyst at 10% conversion of ethane. Under these conditions, 10% of the hydrogen in C_2H_6 was exchanged for deuterium, but the distribution of deuterium in the isotopomers was far from that expected for a binomial distribution. By contrast, the distribution of deuterium in ethene approached that for a binomial distribution. The high fraction of ethene containing deuterium indicates that C_2H_4 once formed readsorbs on the catalyst surface and undergoes H/D exchange. The deuterium content of methane was higher than that expected if all methane were formed by the hydrogenolysis of C_2H_6, supporting the idea that methane is formed by readsorption and subsequent hydrogenolysis of ethene.

The distribution of deuterium in ethane and ethene upon reaction of a C_2H_6/D_2 mixture over PtSn/Mg(Al)O is shown in Fig. 13. The extent of H/D exchange in ethane was only 3% in the case. In contrast to Pt/Mg(Al)O, the extent of H/D exchange into ethene was much lower for PtSn/Mg(Al)O. These results suggest that the addition of Sn to Pt inhibits the readsorption of ethene.

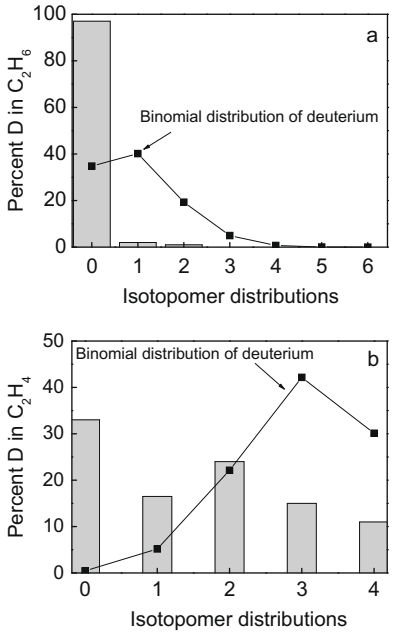

Fig. 13. Isotopomer distribution of (a) $C_2H_xD_{6-x}$ and (b) $C_2H_xD_{4-x}$ observed during ethane dehydrogenation in the presence of D_2 over PtSn/Mg(Al)O (Sn/Pt = 1.08) at 873 K with a C_2H_6 partial pressure of 19.5 kPa, a D_2 feed partial pressure of 11.3 kPa, and a total flow rate of 60 cm^3/min.

3.4. Influence of Sn/Pt ratio on catalyst activity, selectivity, and stability

The effects of Sn/Pt ratio on the activity and selectivity of PtSn/Mg(Al)O is shown in Fig. 14. With increasing Sn/Pt ratio, the rate of production of ethene increases, reaching a maximum at Sn/Pt = 0.3, and then decreases. On the other hand, the selectivity to ethene increases from 60% for Sn/Pt = 0 to nearly 100% for Sn/Pt = 0.6 and then remains constant for higher ratios of Sn/Pt.

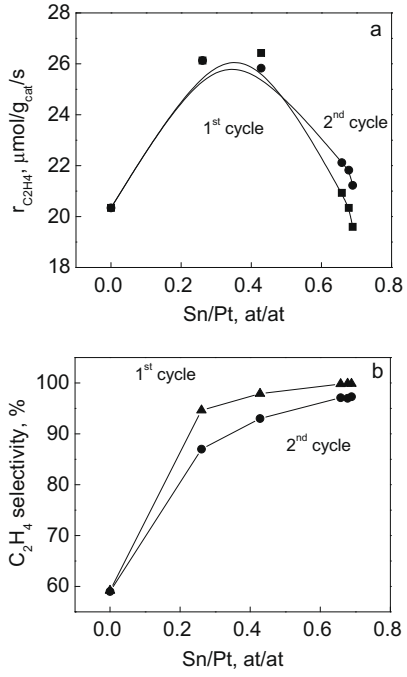

Fig. 14. Effect of Sn/Pt ratio on (a) C_2H_4 product concentration and (b) C_2H_4 selectivity for ethane dehydrogenation on PtSn/Mg(Al)O at 873 K with a C_2H_6 partial pressure of 19.5 kPa, and a total flow rate of 60 cm^3/min.

As noted earlier, both Pt/Mg(Al)O and PtSn/Mg(Al)O undergo noticeable loss in dehydrogenation activity during the first 30 min of time on stream followed by a slower loss in activity for longer reaction times, particularly in the absence of H_2 in the feed. The coke built up during deactivation could be burned off by oxidation at 873 K (see Fig. 8), and the catalyst brought back to its reduced state by treatment in hydrogen at 873 K. As shown in Fig. 14a, there was essentially no change of catalyst activity with regeneration for catalysts prepared with Sn/Pt = 0–0.4, but for higher values of Sn/Pt, the catalyst activity increased slightly with Sn/Pt ratio. A similar increase in activity, but greater in magnitude, after use and regeneration has been reported previously for PtSn/Mg(Al)O catalysts prepared with Sn/Pt > 2 [5,10]. Fig. 14b shows that regeneration of the catalyst also led to a slight decrease in the ethene selectivity.

4. Discussion

The results of this study show that the promotion of Pt/Mg(Al)O with Sn enhances the activity of the catalyst for ethane dehydrogenation and increases the catalyst selectivity to ethene. This effect is strongest for a Sn/Pt ratio of ~0.3. The addition of H_2 to the feed also enhances catalyst activity for the formation of ethene for H_2/C_2H_6 ratio up to about 0.5 but causes a loss in catalyst selectivity for higher H_2/C_2H_6 ratios due to the formation of CH_4. The latter effect is severe for Pt/Mg(Al)O but leads to only a modest loss in selectivity for PtSn/Mg(Al)O. The introduction of Sn also results in a significant reduction in carbon deposition due to coking, as does the addition of H_2 to the feed. Interpretation of these effects is complex, since reactions pathways leading to ethene, methane, and coke are interconnected.

The elementary processes involved in ethane dehydrogenation to ethene, the formation of methane, and the deposition of coke can be described by the following sequence of reactions, in which S_n (n = 1–3) indicates the number of metal atoms interacting with either an H or a C atom.

1. $H_2 + 2S \rightleftharpoons 2H{-}S$
2. $C_2H_6 + 2S \rightarrow C_2H_5{-}S + H{-}S$
3. $C_2H_5{-}S + 2S \rightarrow C_2H_4{-}S_2 + H{-}S$
4. $C_2H_5{-}S + H{-}S \rightarrow C_2H_4{-}S_2 + H_2$
5. $C_2H_4{-}S_2 \rightleftharpoons C_2H_4 + 2S$
6. $C_2H_4{-}S_2 \rightleftharpoons CH_3CH{-}S_2$
7. $CH_3CH{-}S_2 + 2S \rightarrow CH_3C{-}S_3 + H{-}S$
8. $CH_3C{-}S_3 + S \rightarrow CH_3{-}S + C{-}S_3$
9. $CH_y{-}S_{4-y} + (4-y)H{-}S \rightarrow \rightarrow \rightarrow CH_4 + 2(4-y)S$ (y = 1–3)

The dehydrogenation of ethane begins with the dissociative adsorption of C_2H_6 to form C_2H_5–S species (Reaction 2), a reaction that has been observed to occur on Pt(1 1 1) and Pt(1 1 0) surfaces [49–54]. Adsorbed C_2H_4 can form via two competing processes, the first (Reaction 3) involves dissociation of an H atom from C_2H_5–S [49–54]. The second (Reaction 4) involves the attack an adsorbed H atom on C_2H_5–S. While this step has not been proposed in previous studies of ethane dehydrogenation, its involvement is suggested by the results presented in Fig. 8, which show that for H_2/C_2H_6 ratios below 0.58 for Pt/Mg(Al)O and 0.25 for PtSn/Mg(Al)O the formation of ethene is enhanced by increasing the concentration of H_2 in the feed. Ethene and hydrogen are obtained by desorption of C_2H_4–S (Reaction 5) and associative desorption of H_2 (the reverse of Reaction 1). However, adsorbed ethene can also undergo isomerization to form ethylidene, CH_3CH–S_2 (Reaction 6). Dehydrogenation of ethylidene to form ethylidyne, CH_3C–S_3 (Reaction 7). This process is known to occur on Pt, and at temperatures above 400 K, ethylidyne species undergo C–C bond cleavage (Reaction 8) to form CH_y–S_{4-y} species [45,46]. Evidence for the occurrence of Reactions 6–8 on Pt is well documented both experimentally and theoretically [55–62]. In the presence of atomically adsorbed hydrogen, the CH_y–S_{4-y} (y = 1–3) species can undergo hydrogenation to form CH_4 (Reaction 8), whereas dehydrogenation and association of such species very likely contributes to the formation of coke precursors.

It is evident from the proposed reaction mechanism that adsorbed hydrogen plays several important roles. As suggested by Reaction 4, atomically adsorbed hydrogen promotes the dehydrogenation of C_2H_5–S to form C_2H_4–S, adsorbed ethene, via Reaction 4. High H–S coverage is, however, detrimental, since it facilitates the hydrogenation of C_2H_5–S to reform C_2H_6, and the hydrogenation of CH_x–S to form methane via the reverse of Reaction 2 and Reaction 9, respectively. As noted in Fig. 9, H_2/C_2H_6 ratios above 0.58 for Pt/Mg(Al)O and 0.25 for PtSn/Mg(Al)O lead to a decrease in the formation of ethene, the approach of the ethene concentration to that expected for thermodynamic equilibrium, and the formation of increasing amounts of methane. The deposition of coke is also suppressed with increasing feed H_2/C_2H_6 ratio (see Fig. 7). This is envisioned to occur by the reverse of Reaction 7, which leads to a reduction in the surface concentration of coke precursors formed via Reaction 9.

A Bond-order-Morse-Potential (BOC-MP) analysis of Reactions 2–4 reveals that the effect of H_2/C_2H_6 ratio on the formation of C_2H_4 results from the interplay in the kinetics of Reactions 2–4. The activation energy for the forward direction of Reaction 3 is 4 kcal/mol and 0 kcal/mol for the reverse direction of this reaction, whereas the activation for the forward direction of Reaction 4 is 9.5 kcal/mol and 24.5 kcal/mol for the reverse direction [63]. This suggests that an increase in H atom surface concentration will favor the progress of Reaction 4 in the forward direction. An increase in H atom surface concentration also increases the rate of Reaction 2 in the reverse direction, but BOC-MP calculations show that the activation energy for this process is 10 kcal/mol, slightly more than that for Reaction 4 in the forward direction [63]. BOC-MP calculations also suggest that the precursor to C–C bond cleavage is CH_3C–S, since the activation energy for this species to form CH_3–S and C–S, 11 kcal/mol, is significantly lower than that for C–C bond cleavage from any other C_2H_x–S species [63]. This last conclusion is consistent with experimental observations, as noted previously.

The accumulation of coke on the catalyst surface is accompanied by an increase in the selectivity to ethene, as can be seen from Figs. 4 and 5. A similar observation has been reported previously for Pt dispersed on different supports [6,9,27], and this effect has been attributed to a decrease in the presence of large Pt clusters occurring on the surface of Pt particles as coke accumulates on the surface of the Pt particles [9,64].

The addition of Sn to Pt can lead to a variety of bulk and surface structures depending on the Sn/Pt ratio, the nature of the Pt and Sn precursors used, and the manner of catalyst pretreatment [9,14,15,36,65]. Sn oxidation states of 0, +2, and +4 have been observed for supported PtSn catalysts after reduction in H_2. It is generally agreed that Sn(0) is present in bimetallic PtSn particles, whereas Sn(+2) and Sn(+4) are present in the form of SnO and SnO_2 particles, respectively, on the support or in contact with Pt particles. Whereas the phase diagram for PtSn alloys shows stable Pt, Pt_3Sn, PtSn, Pt_2Sn_3, $PtSn_2$, and $PtSn_4$ phases for Sn/Pt ratios of 0 to 4.0 [66], identification of specific PtSn phases in supported PtSn catalysts has proven to be difficult. XPS studies of H_2-reduced PtSn/Mg(Al)O have shown that the metal particles are enriched with Sn for samples prepared with a nominal Sn/Pt ratio of ~ 4; however, the stoichiometry of this phase was not reported [9]. Mössbauer spectroscopy also shows the presence of metallic Sn and Pt–Sn interactions [32,33]. On the other hand, EXAFS evidence for the coexistence particles of

PtSn and Pt phases has been presented for PtSn/SiO_2 and PtSn/γ-Al_2O_3 catalysts, in which Sn was introduced by reaction of $Sn(Bu)_4$ with preformed Pt particles [15], TEM evidence for the formation of Pt_3Sn particles has been reported for PtSn/C [36]. In the present study, selected-area electron diffraction indicates that particles of PtSn were formed upon reduction of as-prepared PtSn/Mg(Al)O (Sn/Pt = 0.23) providing direct evidence for the formation of bimetallic particles. It should be noted, though, that not all of the metal particles have this stoichiometry, and hence it is reasonable to believe that individual metal particles having different Sn/Pt ratios coexist.

As noted previously, the addition of Sn to Pt/Mg(Al)O increases C_2H_6 consumption and the product selectivity to C_2H_4, but diminishes the accumulation of coke, in agreement with the general findings reported earlier for similar catalysts [26]. The present work has also shown (see Fig. 13) that the highest rate of ethane formation occurs for a Sn/Pt ratio of about 0.3. Several hypotheses have been put forth in the literature to explain the means by which Sn alters catalyst properties. The suppression of coke formation by supported by PtSn catalysts has been attributed to both geometric and electronic effects [2,6,16–20,35,67]. The presence of Sn at the surface of PtSn bimetallics reduces the number of adjacent Pt atoms, thereby decreasing the number of Pt atoms in ensembles required to form coke precursors via processes such as Reaction 8 (see above). It has also been found that Sn reduces the heat of adsorption of ethene formed via ethane dehydrogenation [19,24,68]. As noted above, the isotopic tracer studies conducted as a part of this study clearly demonstrate that ethene readsorption is responsible for the formation of CH_x species, the precursors to both methane and coke formation. Sn atoms may also suppress the formation of coke and methane by preferential segregation to step and kink edge sites, where it could attenuate the cleavage of C–C bonds on low-coordination Pt sites exposed at these locations [10].

In contrast to previous studies of ethane dehydrogenation on PtSn/Mg(Al)O [65], the catalysts prepared in the present study were stable to regeneration (see Fig. 13). We believe that this is a consequence of introducing Sn via the selective reaction of $Sn(Bu)_4$ with the Pt particles formed on the support. By contrast, the use of $SnCl_2$ as the precursor for introducing Sn is non-selective and can cause damage to the support since the solution used to introduce Sn in this manner is quite acidic and will react with the basic Mg(Al)O. Moreover, the use of high Sn/Pt ratios (e.g., >2) may result in the formation of $PtSn_2$ particles that have been shown to be less active for ethane dehydrogenation than alloys with lower Sn/Pt ratios [69], and hence the increase in dehydrogenation activity observed with sequential regeneration reported earlier may have been the consequence of the removal of excess Sn from PtSn particles and the storage of Sn on the support as SnO or SnO_2 [65]. Our findings regarding catalyst stability to regeneration are similar to those reported earlier for the promotion of Pt/SiO_2 and Pt/γ-Al_2O_3, in which $Sn(Bu)_4$ was used as the precursor to introduce Sn [15]. In that study PtSn catalysts with Sn/Pt ratios similar to those used in the present work were found to be stable for isobutene dehydrogenation after repeated regeneration by oxidation and reduction.

5. Conclusions

1. Sn promotion of Pt/Mg(Al)O increases the activity of Pt/Mg(Al)O for ethane dehydrogenation to ethene increases for Sn/Pt ratio between 0 and 0.3, beyond which the activity decreases. On the other hand, the selectivity to ethene increases monotonically, and approaches 100% for Sn/Pt ratios above 0.4.
2. Both Pt/Mg(Al)O and PtSn/Mg(Al)O deactivate with time on stream at about the same rate due to the accumulation of coke; however, the amount of coke accumulated on PtSn/Mg(Al)O is significantly lower than that on Pt/Mg(Al)O. Deactivation on both Pt/Mg(Al)O and PtSn/Mg(Al)O is accompanied, though, by an increase in ethene selectivity.
3. Isotopic tracer studies demonstrate that the formation of methane is due primarily to the readsorption of ethene, a process that is much more significant on Pt/Mg(Al)O than on PtSn/Mg(Al)O. Ethene readsorption also contributes to the hydrogenation of ethene to ethane and to the formation of coke precursors.
4. Addition of H_2 to the feed stream increases the product concentration of ethene for H_2/C_2H_6 ratios up to 0.58 for Pt/Mg(Al)O, and ratios of up to 0.25 for PtSn/Mg(Al)O. In both cases, further increases in the H_2/C_2H_6 ratio decreases the product concentration of ethane and enhances the approach to thermodynamic equilibrium. Addition of H_2 of to the feed stream causes a sharp, monotonic decreases in ethene selectivity for Pt/Mg(Al)O, but only a very small decrease in ethene selectivity for PtSn/Mg(Al)O. Coke deposition is also suppressed by H_2 addition to the feed, an effect which is particularly strong for PtSn/Mg(Al)O.
5. The effects of H_2 addition to the feed and Sn promotion of the catalyst can be interpreted in light of the mechanism comprised of Reactions 1–8. This scheme suggests that adsorbed H atoms can promote the dehydrogenation of C_2H_5–S species via Reaction 4. However, a high surface concentration of H atoms is undesirable because it contributes to the hydrogenation of ethene via the reverse of Reaction 4 and to the formation of methane via Reaction 8. H_2 is also envisioned to suppress the formation of C_2H_x–S_2 species, which are the precursors to CH_y–S species formed via Reaction 7. The latter species are undesirable, since they can undergo hydrogenation to form methane as well dehydrogenation to form coke. Promotion of Pt/Mg(Al)O with Sn suppresses the readsorption of ethene thereby inhibiting hydrogenation of the ethene back to ethane and the contribution of adsorbed ethene to the formation of methane and coke.
6. Coke accumulated on either Pt/Mg(Al)O or PtSn/Mg(Al)O can be fully removed by oxidation, and the catalyst activity restored by subsequent reduction. Regeneration by such treatment appears to have little effect on the activity of catalysts prepared with Sn/Pt ratios less than ~0.3, and leads to a slight improvement in ethene formation activity for higher Sn/Pt ratios. Regeneration, however, leads to small loss in ethene selectivity independent of the Sn/Pt ratio.

Acknowledgments

This work was supported by a grant from Chevron Energy and Technology Company. The HRTEM work was performed at NCEM, which is supported by the Office of Science, Office of Basic Energy Sciences of the US Department of Energy under Contract No. DE-AC02-05CH11231.

References

[1] F. Cavani, N. Ballarini, A. Cericola, Catalysis Today 127 (2007) 113–131.
[2] D. Sanfilippo, I. Miracca, Catalysis Today 111 (2006) 133–139.
[3] M.M. Bhasin, J.H. McCain, B.V. Vora, T. Imai, P.R. Pujadó, Applied Catalysis A: General 221 (2001) 397–419.
[4] S. de Miguel, A. Castro, O. Scelza, J.L.G. Fierro, J. Soria, Catalysis Letters 36 (1996) 201–206.
[5] D. Akporiaye, S.F. Jensen, U. Olsbye, F. Rohr, E. Rytter, M. Ronnekleiv, A.I. Spjelkavik, Industrial & Engineering Chemistry Research 40 (2001) 4741–4748.
[6] R.D. Cortright, J.M. Hill, J.A. Dumesic, Catalysis Today 55 (2000) 213–223.

[7] H. Armendáriz, A. Guzmán, J.A. Toledo, M.E. Llanos, A. Vázquez, G. Aguilar-Rìos, Applied Catalysis A: General 211 (2001) 69–80.
[8] F. Cavani, F. Trifirò, A. Vaccari, Catalysis Today 11 (1991) 173–301.
[9] A. Virnovskaia, S. Jørgensen, J. Hafizovic, Ø. Prytz, E. Kleimenov, M. Hävecker, H. Bluhm, A. Knop-Gericke, R. Schlögl, U. Olsbye, Surface Science 601 (2007) 30–43.
[10] A. Virnovskaia, S. Morandi, E. Rytter, G. Ghiotti, U. Olsbye, The Journal of Physical Chemistry C 111 (2007) 14732–14742.
[11] O.A. Bariås, A. Holmen, E.A. Blekkan, Journal of Catalysis 158 (1996) 1–12.
[12] M. Santhosh Kumar, D. Chen, J.C. Walmsley, A. Holmen, Catalysis Communications 9 (2008) 747–750.
[13] S.A. Bocanegra, A.A. Castro, O.A. Scelza, S.R. de Miguel, Applied Catalysis A: General 333 (2007) 49–56.
[14] C. Kappenstein, M. Guérin, K. Lázár, K. Matusek, Z. Paál, Journal of the Chemical Society, Faraday Transactions 94 (1998) 2463–2473.
[15] G.J. Siri, J.M. Ramallo-López, M.L. Casella, J.L.G. Fierro, F.G. Requejo, O.A. Ferretti, Applied Catalysis A: General 278 (2005) 239–249.
[16] S. Scirè, G. Burgio, C. Crisafulli, S. Minicò, Journal of Molecular Catalysis A: Chemical 260 (2006) 109–114.
[17] R.J. Rennard, J. Freel, Journal of Catalysis 98 (1986) 235–244.
[18] W.A.G.J. Kua, Journal of Physical Chemistry B 103 (1999) 2318.
[19] Y.-L. Tsai, B.E. Koel, Journal of Physical Chemistry B 101 (1997) 2895–2906.
[20] M. Batzill, D.E. Beck, B.E. Koel, Surface Science 466 (2000) L821–L826.
[21] J.M. Ramallo-López, G.F. Santori, L. Giovanetti, M.L. Casella, O.A. Ferretti, F.G. Requejo, The Journal of Physical Chemistry B 107 (2003) 11441–11451.
[22] R. Alcala, J.W. Shabaker, G.W. Huber, M.A. Sanchez-Castillo, J.A. Dumesic, The Journal of Physical Chemistry B 109 (2005) 2074–2085.
[23] J.M. Essen, J. Haubrich, C. Becker, K. Wandelt, Surface Science 601 (2007) 3472–3480.
[24] J. Shen, J.M. Hill, R.M. Watwe, B.E. Spiewak, J.A. Dumesic, The Journal of Physical Chemistry B 103 (1999) 3923–3934.
[25] E. Janin, H. von Schenck, S. Ringler, J. Weissenrieder, T. Åkermark, M. Göthelid, Journal of Catalysis 215 (2003) 245–253.
[26] A. Virnovskaia, E. Rytter, U. Olsbye, Industrial & Engineering Chemistry Research 47 (2008) 7167–7177.
[27] C. Yu, Q. Ge, H. Xu, W. Li, Industrial & Engineering Chemistry Research 46 (2007) 8722–8728.
[28] M. Tasbihi, F. Feyzi, M.A. Amlashi, A.Z. Abdullah, A.R. Mohamed, Fuel Processing Technology 88 (2007) 883–889.
[29] S.B. Kogan, H. Schramm, M. Herskowitz, Applied Catalysis A: General 208 (2001) 185–191.
[30] H.H.C.M. Pinxt, B.F.M. Kuster, D.C. Koningsberger, G.B. Marin, Catalysis Today 39 (1998) 351–361.
[31] E. Merlen, P. Beccat, J.C. Bertolini, P. Delichère, N. Zanier, B. Didillon, Journal of Catalysis 159 (1996) 178–188.
[32] C. Vértes, E. Tálas, I. Czakó-Nagy, J. Ryczkowski, S. Göbölös, A. Vértes, J. Margitfalvi, Applied Catalysis 68 (1991) 149–159.
[33] R.D. Cortright, J.A. Dumesic, Journal of Catalysis 148 (1994) 771–778.
[34] N. Nava, P. Del Angel, J. Salmones, E. Baggio-Saitovitch, P. Santiago, Applied Surface Science 253 (2007) 9215–9220.
[35] L. Bednarova, C.E. Lyman, E. Rytter, A. Holmen, Journal of Catalysis 211 (2002) 335–346.
[36] V. Radmilovic, T.J. Richardson, S.J. Chen, P.N. Ross Jr., Journal of Catalysis 232 (2005) 199–209.
[37] E. Antolini, F. Colmati, E.R. Gonzalez, Journal of Power Sources 193 (2009) 555–561.
[38] M. Womes, J. Lynch, D. Bazin, F. Le Peltier, S. Morin, B. Didillon, Catalysis Letters 85 (2003) 25–31.
[39] J. Margitfalvi, M. Hegedus, S. Gobolos, E. Kern-Talas, P. Szedlacsek, S. Szabo, F. Nagy, Controlled surface reaction for preparation of Sn–Pt/Al_2O_3 catalysts, in: Proc. of 8th Intl. Congress on Catalysis, Berlin, 1984, p. 903.
[40] F. Humblot, F. Lepeltier, J.P. Candy, J. Corker, O. Clause, F. Bayard, J.M. Basset, Journal of the American Chemical Society 120 (1998) 137–146.
[41] http://www.totalresolution.com.
[42] G.L. Price, E. Iglesia, Industrial & Engineering Chemistry Research 28 (2002) 839–844.
[43] U. Costantino, F. Marmottini, M. Nocchetti, R. Vivani, European Journal of Inorganic Chemistry 1998 (1999) 1439–1446.
[44] J.A.v. Bokhoven, J.C.A.A. Roelofs, K.P.d. Jong, D.C. Koningsberger, Chemistry 7 (2001) 1258–1265.
[45] P. Villars, L.D. Calvert, W.B. Pearson, Pearson's Handbook of Crystallographic Data for Intermetallic Phases, ASM International, Materials Park, Ohio, 1991.
[46] S.M.K. Airaksinen, M.A. Bañares, A.O.I. Krause, Journal of Catalysis 230 (2005) 507–513.
[47] D. Espinat, H. Dexpert, E. Freund, G. Martino, M. Couzi, P. Lespade, F. Cruege, Applied Catalysis 16 (1985) 343–354.
[48] F. Tuinstra, J.L. Koenig, The Journal of Chemical Physics 53 (1970) 1126–1130.
[49] S.M. Davis, G.A. Somojai, Hydrocarbon Conversion over Metal Surfaces, Elsevier Scientific, Amsterdam, 1982.
[50] D.J. Oakes, H.E. Newell, F.J.M. Rutten, M.R.S. McCoustra, M.A. Chesters, Chemical Physics Letters 253 (1996) 123–128.
[51] J.F. Weaver, M.A. Krzyzowski, R.J. Madix, The Journal of Chemical Physics 112 (2000) 396–407.
[52] M.C. McMaster, S.L.M. Schroeder, R.J. Madix, Surface Science 297 (1993) 253–271.
[53] J.J.W. Harris, V. Fiorin, C.T. Campbell, D.A. King, The Journal of Physical Chemistry B 109 (2005) 4069–4075.
[54] C.R. Arumainayagam, G.R. Schoofs, M.C. McMaster, R.J. Madix, The Journal of Physical Chemistry 95 (2002) 1041–1047.
[55] P.K. Wang, C.P. Slichter, J.H. Sinfelt, The Journal of Physical Chemistry 89 (1985) 3606–3609.
[56] P.-K. Wang, J.-P. Ansermet, S.L. Rudaz, Z. Wang, S. Shore, C.P. Slichter, J.H. Sinfelt, Science 234 (1986) 35–41.
[57] Q. Ge, D.A. King, The Journal of Chemical Physics 110 (1999) 4699–4702.
[58] G.W. Watson, R.P.K. Wells, D.J. Willock, G.J. Hutchings, The Journal of Physical Chemistry B 104 (2000) 6439–6446.
[59] G. Papoian, J.K. Norskov, R. Hoffmann, Journal of the American Chemical Society 122 (2000) 4129–4144.
[60] A.T. Anghel, S.J. Jenkins, D.J. Wales, D.A. King, The Journal of Physical Chemistry B 110 (2006) 4147–4156.
[61] A.T. Anghel, D.J. Wales, S.J. Jenkins, D.A. King, The Journal of Chemical Physics 126 (2007) 044710–044713.
[62] A.V. Zeigarnik, R.E. Valdes-Perez, O.N. Myatkovskaya, The Journal of Physical Chemistry B 104 (2000) 10578–10587.
[63] A.T. Bell, E. Shustorovich, Surface Science 235 (1990) 343–350.
[64] Z. Tian, Y. Xu, L. Lin, Chemical Engineering Science 59 (2004) 1745–1753.
[65] N.A. Pakhomov, Kinetics and Catalysis 42 (2001) 334–343.
[66] X. Su, F. Yin, M. Huang, Z. Li, C. Chen, Journal of Alloys and Compounds 325 (2001) 109–112.
[67] J. Llorca, N. Homs, J. León, J. Sales, J.L.G. Fierro, P. Ramirez de la Piscina, Applied Catalysis A: General 189 (1999) 77–86.
[68] R.M. Watwe, R.D. Cortright, M. Mavrikakis, J.K. Norskov, J.A. Dumesic, The Journal of Chemical Physics 114 (2001) 4663–4668.
[69] R.A. Buyanov, N.A. Pakhomov, Kinetics and Catalysis 42 (2001) 64–75.